Nuclear magnetic resonance analysis of the failure and damage model of rock masses during freeze−thaw cycles

Taoying Liu[1] · Mengyuan Cui[1] · Chaoyang Zhang[1] · Keping Zhou[1] · Wenchao Shi[1] · Ping Cao[1]

Abstract

Multiple freeze–thaw cycle tests were conducted on sandstone samples. The sandstone samples were examined using X-ray diffraction (XRD) and nuclear magnetic resonance (NMR). The mineral content, porosity distribution, T_2 (transverse relaxation time) spectral distribution, spectral area, and nuclear magnetic resonance imaging (MRI) data for sandstone samples were obtained, and the distribution and variation of the sample pores were analyzed. Uniaxial compression tests were performed on samples that had undergone 0, 20, 40, and 80 freeze−thaw cycles, and the effects of freeze−thaw cycles on the mass, compressive strength, and elastic modulus of the sample were analyzed. The damage evolution and strength degradation characteristics of sandstone after freeze−thaw cycles were studied. As the number of freeze−thaw cycles increases, mineral particle flaking and cracking appear on the rock surface, the uniaxial compressive strength and elastic modulus of rock samples decrease, and the typical stress–strain curve compaction stage corresponding to the deformation increases. According to the NMR T_2 distribution, the pore size of rock samples increases after 80 freeze−thaw cycles, especially that of medium-sized and small-sized pores. Meanwhile, the internal damage to the rock mass is a gradual process of cumulative fatigue damage caused by freezing and thawing, and the microscopic damage evolution law during freeze−thaw cycles was revealed using MRI. Based on plasticity theory and damage fracture mechanics theory, the sandstone damage propagation criterion under freeze−thaw-loading action was deduced, and a sandstone freeze−thaw damage degradation model was established.

Keywords Freeze–thaw cycles · Nuclear magnetic resonance · Strength deterioration · Damage evolution · Porosity distribution · Damage model

Introduction

As geotechnical engineering and construction in cold areas gradually progresses, an increasing number of engineering problems are encountered, among which the effect of freeze–thaw cycles on the mechanical properties of rock masses constitutes one engineering research focus. Many slopes, bridges and building foundations, culverts, and tunnels face freeze−thaw problems (Liu et al. 2019a; Xu et al. 2020; Wang et al. 2021b), especially in cold and high altitude areas, where the hazard of freeze–thaw cycles to engineering is more significant. The long-term durability of rock under severe climatic conditions is a key determinant of the stability of rockwork and natural stone as a building material. Several studies have shown functional damage due to icing and frost damage in countries such as Austria, Germany, Norway, China, and Japan (Kellerer-Pirklbauer 2017; Ishikawa and Kawabata 2016; Li et al. 2020; Park et al. 2020; Lindner et al. 2021). The pore water in the rock produces a freezing expansion force that expands the volume of the water by approximately 9%, and this pressure gradually disappears when the ice melts. Frequent freeze−thaw cycles of pore water inside the rock expand cracks and pores, promoting the development of new microcracks (Park et al. 2015; Liu et al. 2020a, 2021a; Li et al. 2021); the continued development of these microcracks may lead to geotechnical damage. Freeze–thaw damage of rocks is an irreversible deformation process caused by this cyclic freeze-expansion pressure in alternating cold and warm climates, which may lead to rapid strength degradation and pose a hazard to rock works and buildings (Luo et al. 2015; Amin et al. 2016; Liu et al. 2021b). An analysis of the pore structure deterioration characteristics of rocks under the action of freeze–thaw

✉ Taoying Liu
 taoying@csu.edu.cn

1 School of Resources & Safety Engineering, Central South University, Changsha, Hunan 410083, China

cycles may help reveal the damage mechanism of rocks in cold areas, which has significant value in construction projects in cold areas.

Scholars have conducted extensive research on the mechanical properties of rocks in cold regions. These studies include the freeze–thaw cycle temperature (Gao et al. 2019; Yuan et al. 2021), number of freeze–thaw cycles (Wang et al. 2020b; Guo et al. 2022), rock water content (Al-Omari et al. 2015; Wang et al. 2021a), chemical environment (Li et al. 2019a; Wang et al. 2020a), and other aspects. Momeni et al. (2016) conducted long-term freeze–thaw experiments on granite to determine its P-wave velocity, porosity, water absorption, dry density, uniaxial compressive strength, and tensile strength. The results showed that as the number of freeze–thaw cycles increased, the uniaxial compressive strength, tensile strength, dry density, and P-wave velocity decreased, while water absorption and porosity increased. The aforementioned studies focus primarily on macroscopic damage in rocks. Liu et al. (2020b) performed high-precision computed tomography (CT) scans to study the mesoscopic structure and damage characteristics of sandstone and clearly observed particle detachment, crack sprouting, crack extension, and porosity increase due to water volume expansion inside the rock. Sokhansefat et al. (2020) investigated the role of critical saturation (DOS) and void systems on crack expansion in Portland cement mortars subjected to freeze–thaw cycles using X-ray scanning and observed that cracks that appeared prior to freeze–thaw cycles expanded and new cracks started at the slurry-aggregate interface. Abdolghanizadeh et al. (2020) studied the effects of freeze–thaw cycles and freezing temperature on the type I and type II fracture toughness of the Lushan sandstone using X-rays and found that the mode I and mode II fracture toughness showed a nonlinear decreasing trend with the increase in the number of freeze–thaw cycles. The type I and type II fracture toughness of the Lushan sandstone showed a nonlinear decreasing trend with increasing freezing temperature during freeze–thaw cycles. Su et al. (2021) conducted a series of freeze–thaw cycling experiments and triaxial compressional acoustic emission (AE) tests on granite samples using the monitoring function of the AE technique and found that the longitudinal wave velocity and peak intensity of acoustic emission of granite showed a significant decreasing trend with the increase in the number of freeze–thaw cycles. The peak frequency distribution tended to change from high to low with the increase in the number of freeze–thaw cycles. Zhou et al. (2020) conducted scanning electron microscopy (SEM) tests to study the evolution of the microstructure of sandstone at the same location under freeze–thaw cycles and found that the cycles caused significant grain exfoliation in the samples. The nuclear magnetic resonance (NMR) technique has been applied to experimental studies exploring the pore distribution and internal structural features of rocks (Li et al. 2016; Li et al. 2019b; Liu et al. 2019b). In addition, the pore distribution

characteristics of solid porous media have been visualized using magnetic resonance imaging (MRI) (Liu et al. 2021c), which is a useful method to study the fractal characteristics of rock microstructures. Based on numerical simulation software, Wang et al. (2019) developed an improved hybrid finite element method (FEM) to study the stability of surrounding fractured rocks. Meng et al. (2022) proposed a numerical model based on the finite element-cohesive zone model (FEM-CZM) method to investigate the fracture pattern and fracture characteristics of mudstone in detail. The numerical results showed that BPS, lamina face spacing, and location exert substantial effects on the type I fracture characteristics of short transverse specimens. Peng et al. (2019) used two methods to investigate whether the initial microcrack damage produced under different loading conditions affected the simulation results. In method 1, the numerical model was loaded vertically to different stresses and then unloaded to a zero stress level. In method 2, different loading/unloading cycles were performed to produce numerical models with different levels of initial microcrack damage. Zhou et al. (2022) investigated the deformation and damage laws of biaxial and triaxial tensile stress granite material models using the numerical simulation software CAS-Rock. The tensile strength of granite decreased with increasing surrounding pressure. As shown in previous macroscopic or microscopic studies, actual experiments, or numerical simulations, the combination of macroscopic and microscopic results is less, and the error is relatively large compared to the natural state. Freeze–thaw cycling experiments are performed while comprehensively considering macroscopic and microscopic defects, with the simulated environment closer to natural conditions. Using the nondestructive properties of NMR technology, the same specimen can be tracked and examined during freeze–thaw cycles to obtain a more accurate understanding of the pattern of changes in the internal structure of the specimen.

In the present study, a series of freeze–thaw cycle tests is conducted on sandstone samples, and NMR spectroscopy is used to measure the rock microstructure. The microstructure and macroscopic characteristics of rock samples after freeze–thaw cycles are studied. The results of the mass, porosity, and T_2 distribution of rock during freeze–thaw cycles are evaluated and discussed, and a model of freeze–thaw degradation of rock mass based on the change in the relative elastic modulus is established.

Experimental design

XRD experiment

The porosity of sandstone is relatively high, and the connectivity of pores is good, suggesting that the material is more suitable for laboratory experiments. The rock samples are shown in Fig. 1. The red sandstone is brownish red, with a

fine texture and uniform particle size distribution. According to the results of X-ray diffraction (XRD) analysis (Fig. 2), the main components are quartz and calcite, along with other minor minerals, such as hematite, albite, and muscovite.

By comparing XRD patterns, the chemical formula of the relevant mineral components was identified, and the percentage of mineral components of the sandstone sample was calculated, as shown in Table 1.

NMR technology

Nuclei have magnetic moment and spin characteristics. In reaction to an external magnetic field, these spinning and magnetic nuclei will move in the direction of the external magnetic field. The interaction between the nucleus and the external magnetic field will generate a signal that is detected using a special coil (Li 2012). The nucleus is composed of charged protons and uncharged neutrons, and when one or both of the number of neutrons and protons in the nucleus are odd, the nucleus will exhibit spin characteristics and subsequently generate MRI signals. In nature, many nuclei with spin characteristics have been observed, among which hydrogen atoms have a proton, and abundant hydrogen nuclei are present in nature with high detection sensitivity and a large magnetic moment. Therefore, NMR core detection is used to detect the relaxation characteristics of hydrogen-containing fluids in pores. The sample is placed into a specific magnetic field and subjected to radio frequency pulses with a certain frequency. The hydrogen proton will absorb the energy of the radio frequency pulses and generate nuclear magnetic resonance. When the RF pulse ends, the hydrogen proton will release the energy it has just absorbed, and a specific coil is used to detect the energy released from
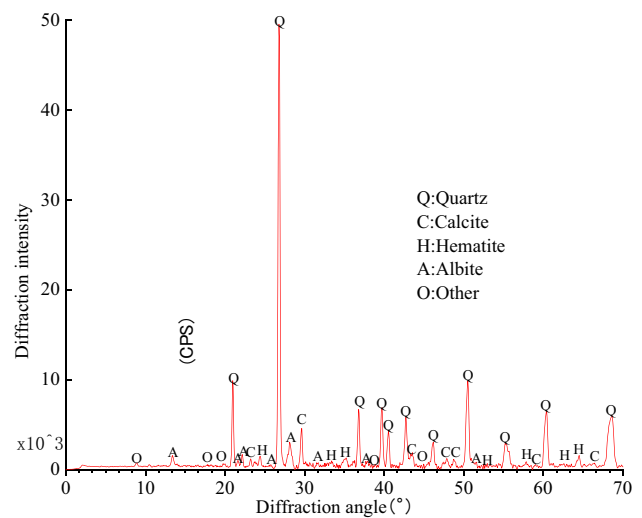

Fig. 1 Rock sample

Fig. 2 XRD pattern of red sandstone

hydrogen protons, which is known as an NMR signal. Due to the different properties of the sample, the radio-frequency pulse energy is released at different speeds, which is reflected in different NMR signals. By detecting different NMR signals, the change in the pore structure of the rock can be directly determined.

T_2 is a time constant describing the decay of the transverse component of magnetization. According to NMR theory, the transverse relaxation rate of nuclear magnetic resonance is calculated using the following equation (Coates et al. 2007):

$$\frac{1}{T_2} = \frac{1}{T_2^1} + \frac{\rho_2 s}{V} + \frac{D(\gamma G T_E)^2}{12} \tag{1}$$

where T_2^1 is the relaxation time of the fluid, ρ_2 is the transverse surface relaxation strength, s is the pore surface area, V is the pore volume, $\frac{\rho_2 s}{V}$ is the transverse surface relaxation rate, D is the diffusion coefficient, γ is the gyromagnetic ratio, G is the gradient of the magnetic field, T_E is the echo time, and $\frac{D(\gamma G T_E)^2}{12}$ is the diffusion relaxation rate.

In the present study, only one type of fluid (water) is present in the pores, and the volume relaxation is much slower than that of the area; therefore, $\frac{1}{T_2^1}$ is ignored. When the magnetic field is even and the T_E adopted is short, the diffusion relaxation is also ignored. Therefore, Eq. (1) can be simplified as follows:

Table 1 Percentages of minerals contained in the red sandstone sample

Mineral composition	Quartz	Albite	Hematite	Calcite	Other
Mass percentage/%	67.805	17.339	3.869	9.960	1.027

$$\frac{1}{T_2} = \frac{1}{T_2^1} + \frac{\rho_2 s}{V} \tag{2}$$

In Eq. (2), the rate of transverse relaxation depends on the surface-to-volume ratio of the pores. Thus, the T_2 distribution indicates the pore size: the smaller the T_2 value is, the smaller the pore size is, and the larger the T_2 value is, the larger the pore size is.

Experimental procedures

Experiment preparation

Red sandstone collected from the cold region in western China was used in this experiment. All samples were collected from the same fresh rock to ensure the uniformity of the samples and the comparability of the test data. Five groups of freeze–thaw cycle tests, including 0, 20, 40, 60, and 80 cycles, were conducted to study the physical characteristics, porosity, NMR T_2 spectrum, and mechanical characteristics of the rock masses after different freeze–thaw cycles and to analyze the evolution of freeze–thaw damage and strength degradation of the rock mass.
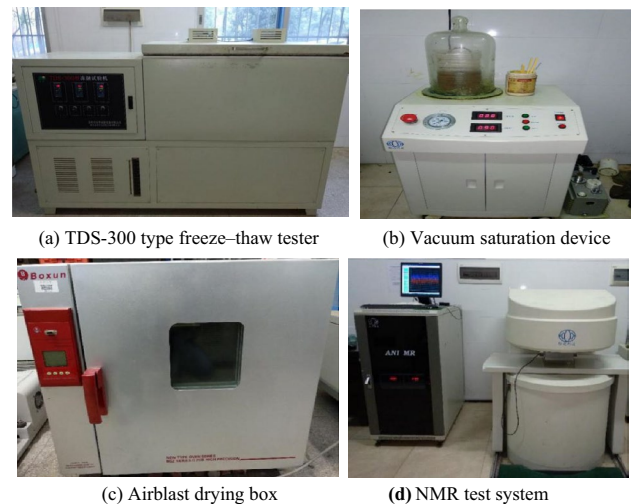
The core was removed from a large red sandstone block using an automatic coring machine to ensure the representativeness and identity of the prepared rock samples and avoid the effects of original defects inside the original rock. The rock samples were prepared as cylinders with a diameter of 50 mm and a height of 100 mm. The roughness error of the two ends of the sample was not greater than 0.05 mm. The errors in height and diameter were within 0.3 mm. The main test equipment included a TDS-300-type freeze–thaw test, vacuum saturation device, air blast drying box, and NMR test system, as shown in Fig. 3.

The mechanical parameters of the red sandstone used in the experiment are shown in Table 2.

Freeze–thaw test

Changes in NMR-measured porosity, the T_2 spectrum, and other physical properties and mechanical parameters of the rock mass were obtained after 0–80 freeze–thaw cycles. The specific test scheme is described below.

1. The height, diameter, quality, and porosity of the saturated samples were tested.
2. The mass, surface features, diameter, height, and NMR properties of the saturated sample were measured after every 20 freeze–thaw cycles. The nuclear magnetic resonance measurements included a porosity measurement, T_2 spectral distribution, and T_2 spectral area change. After 80 cycles, the freeze–thaw test was complete.

(a) TDS-300 type freeze–thaw tester   (b) Vacuum saturation device

(c) Airblast drying box   (d) NMR test system

Fig. 3 Main test equipment. **a** TDS-300 type freeze–thaw tester. **b** Vacuum saturation device. **c** Airblast drying box. **d** NMR test system

3. After a defined number of cycles (0/20/40/60/80 times), a uniaxial compression mechanics test was performed to obtain the corresponding physical parameters, and the displacement control mode was adopted with a loading rate of 0.2 mm/min.

Before freezing and thawing, all rock samples were treated and saturated with water. After thawing, excess water in the test box was drawn out automatically for freezing. All instructions and parameters were preset through the control panel at the front of the machine before the freeze–thaw cycle test. The specific parameters were 360 min of freezing time, 360 min of melting time, 3 min of water intake, and 4 min of pumping time. The cooling slope was 0.5 °C. The target freezing temperature was –20 °C, and the target melting temperature was 20 °C. Through real-time observations of the changes in parameters using the secondary program controller, which is located at the front end of the freezing and thawing test machine, approximately 1.5 h was required for the temperature of the freeze–thaw test chamber to decrease from room temperature (20 °C) to -20 °C. Similarly, 1.5 h were required for the freeze–thaw test chamber to heat from –20 to 20 °C. The total duration of a freeze–thaw cycle was 15 h.

Table 2 Basic physical parameters of the rock sample

Dry density $\rho_d/g \cdot cm^{-3}$	Saturated density $\rho_s/g \cdot cm^{-3}$	Natural moisture content $\omega_0/\%$	Saturation moisture content $\omega_s/\%$	Longitudinal wave velocity $v_p/m \cdot s^{-1}$	Porosity $n_0/\%$
2.39	2.46	1.16	3.57	2962	5.35

The temperature curve for the freezing and thawing cycles is shown in Fig. 4.

According to the temperature change curve of the freeze–thaw cycle, the freeze–thaw cycle is divided into four stages: cooling stage, freezing stage, heating stage, and melting stage. The cooling and heating stages exhibit approximately parabolic changes. This property can be attributed to the greater work required by the refrigerating compressor in the cooling stage, when the temperature drops from normal temperature to freezing temperature, and the temperature decreases more slowly at the same time. Therefore, the temperature decreases more rapidly in the early stage of cooling and gradually slows after reaching the freezing point. In the heating process, when the freezing stage is complete, the test machine will automatically pour water into the freeze–thaw test box. Consequently, the frozen rock sample melts rapidly, and the temperature of the freeze–thaw test box increases. In the heating stage, the temperature in the early stage increases more rapidly. As the temperature of the rock approaches the temperature of the water, the temperature of the test chamber reaches equilibrium and then increases more slowly.

Correspondingly, the freeze–thaw damage and deformation characteristics of the rock at each stage are not consistent. In Fig. 4, the cooling stage is divided into two phases: the normal temperature is reduced to 0 °C, and the 0 °C temperature is lowered to the target freezing temperature. As the temperature decreases to the freezing point, the volume of the skeleton particles inside the rock will shrink due to the decrease in temperature, but since the temperature is always higher than the freezing point temperature, no frost heaving force will occur, and the deformation of the rock will thus be small. In the latter phase, when the temperature is lowered to a certain extent, the volume expands after the rock is saturated due to certain defects in the rock. The larger

the pores inside the rock are, the higher the water content is after the rock is saturated, and the more obvious the volume expansion is after freezing. These effects can be attributed to the expansion in the volume of water as it becomes ice when the temperature is lower than the freezing point, and the rock will undergo frost heaving damage. As the temperature of the rock decreases to –20 °C, the deformation rate of the rock tends to gradually stabilize during the freezing stage. After the freezing stage, the rock sample enters the melting phase, which includes the two stages of heating and melting. The heating stage also corresponds to two phases in which the negative temperature increases to 0 °C, followed by an increase from 0 °C to the target melting temperature. As the temperature increases from –20 to 0 °C, the frost heave deformation of the rock sample remains unchanged at the initial stage. As the temperature increases further, damage will occur between the rock particles, the volume of the rock will expand, the ice inside the rock will melt, and the frost heaving force will slowly disappear. During the heating process from 0 °C to the target temperature, the ice crystals inside the rock continuously melt to form water as the temperature rises. The pressure of the ice on the rock fissure wall decreases, the water penetrates through the pores or capillary channels, and the damage increases with the change in temperature. When the melting stage is complete, a freeze–thaw cycle is complete, and the next freeze–thaw cycle is performed. Repeated freeze–thaw cycles will induce fatigue damage in the rock and eventually lead to rock damage (Liu et al. 2020b).

Results

Macroscopic deterioration caused by freeze–thaw cycles

Change in quality

The masses of the three rock samples G1-1–G1-3 were measured after each freeze–thaw target was completed. The average quality of the sample was compared with the quality of the 0-cycle saturated sample after every 20 freeze–thaw cycles to study the change in the quality of the sample after different numbers of freeze–thaw cycles. The comparison is shown in Table 3.

As shown in Table 3, the average mass of rock shows an increasing trend before the 20 freeze–thaw cycles. After 20 freeze–thaw cycles, the quality of the samples generally shows a decreasing trend. The reason is that the red sandstone is a medium hard rock. As the number of freeze–thaw cycles increases, the top of the saturated rock alternates between freezing and melting. When the rock is in the freezing stage, the temperature of the outside of the rock is lower
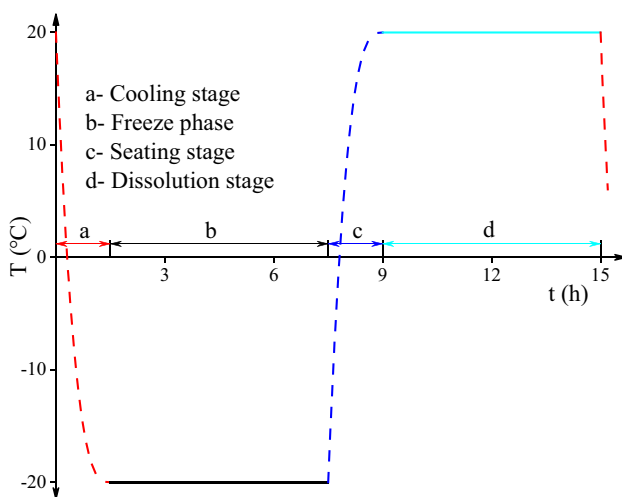
Fig. 4 Schematic of the temperature change in the freeze–thaw cycle

Table 3 Mass and mass change rate of sandstone samples after different numbers of freeze–thaw cycles

Sample number	Quality/g				
	0 cycle	20 cycles	40 cycles	60 cycles	80 cycles
G1-1	474.68	475.53	472.89	471.75	466.20
G1-2	478.66	472.89	476.54	475.01	470.75
G1-3	486.21	487.42	485.86	477.09	472.03
Average	479.85	480.32	478.43	476.05	469.66
Rate of change/%	0	0.37	–0.32	–0.79	–2.12

than that inside when the temperature of the rock decreases to –20 °C. There is a thin layer of unfrozen water film between the mineral particles and the ice crystal. The water film separates the rock mineral particles from the ice crystals and continuously attracts the unfrozen water to the unfrozen water film. Therefore, tension is generated that accelerates damage to the sand at the top of the rock. Before 20 freeze–thaw cycles, new microcracks occur at the top of the rock due to freeze–thaw damage. When the rock is saturated, water slowly migrates to the newly expanded microcracks, and the rock volume increases. With the increase in the number of freeze–thaw cycles, the mineral particles inside the rock will dislocate through the effects of the water–ice phase change and ice-water phase change, and fragment or particle shedding will occur at the top of the sample, decreasing the quality of the rock sample.

Sandstone degradation

With the increase in the number of freeze–thaw cycles, the samples showed different degrees of appearance damage and deformation (as shown in Fig. 5). After 20 freeze–thaw cycles, the mineral particles at the edge of the radial end face of the rock sample become loose and frozen. A small amount of mineral particles is observed at the bottom of the test chamber. After 40 freeze–thaw cycles, the mineral particles are peeled off at the edge of the end face of the rock sample, and tiny pores appear in the sample. After 60 cycles, the mineral particles are peeled off at the edge of the end of the rock sample, and tiny pores are observed on the surface of the sample. After 80 cycles, the spalling of the mineral particles at the edge of the end face is accelerated, scattered mineral particles are present in the freeze–thaw test box and the saturated container, and the local area of the sample can be crushed by hand.

By tracking and recording the apparent changes in each group of samples in the freeze–thaw cycle test, the freeze–thaw damage degradation mode of the rock mass appears as the spalling of mineral particles: in the freezing

Fig. 5 Apparent changes in the sample during freeze–thaw cycles

stage, the surface of the rock reaches the freezing point first. Due to the volume expansion of the water–ice phase change, a frost heaving force is generated. As the temperature gradually decreases to the target freezing temperature of –20 °C, the low temperature is transmitted from the surface of the rock to the inside of the rock. Due to the driving force of the condensing potential, free water will migrate to the freezing edge, resulting in an increase in the ice volume. In the melting stage, the outside of the rock first reaches the freezing point temperature, and the external water will undergo the opposite process, moving from the outside to the inside. Repeated freezing and thawing will weaken the bonding force of the cemented particles in the rock structure, and the microcracks will increase. At the same time, phenomena such as scattering, peeling, and softening of the mineral particles will occur on the surface of the sample. These phenomena will become increasingly obvious as the number of cycles increases.

NMR characteristics

NMR T_2 spectral curve distribution

Through NMR analysis of rock samples, the pore structure characteristics of sandstone are characterized by measuring and analyzing the T_2 spectrum distribution. The T_2 spectral distribution reflects the pore size of the sandstone: the smaller the T_2 value is, the smaller the pore size is, and the larger the T_2 value is, the larger the pore size is. At the same time, the change in the T_2 spectrum distribution before and after freezing and thawing reflects the change in pores. Transversely, the

left and right movement of the curve represents the decrease and increase in pore size, respectively. Vertically, the increase and decrease in the amplitude of the curve represent the increase and decrease in the number of pores, respectively.

Different pore sizes are divided by referring to similar studies to quantify the variation in various types of pore sizes. In the literature (Zhou et al. 2015), the T_2 spectral curve of marble is divided into different pore types according to the T_2 values of different spectral peaks. The first peak is a small pore, and the peak corresponding to the largest T_2 value is a large pore. Li et al. (2014) and Yao et al. (2010) also proposed similar pore division methods for T_2 spectrum peak values. According to the analysis of the NMR T_2 spectrum of sandstone, the T_2 spectrum contains three peaks with distribution times of 0.5–2, 8–12, and more than 100 ms. The three peaks correspond to micropores and transition pores (< 100 nm), mesopores (100–1000 nm), and macropores or microcracks. Figure 6 shows a typical T_2 spectrum distribution and pore size distribution of sandstone.

The different types of apertures were quantified. The calculation boundary of different aperture types is based on the lowest point between the peaks, namely the end time point of the first peak and the start time node of the second peak for T_2 spectrum accumulation statistics. The critical point of the second spectrum peak is the same as that of the third spectrum peak.
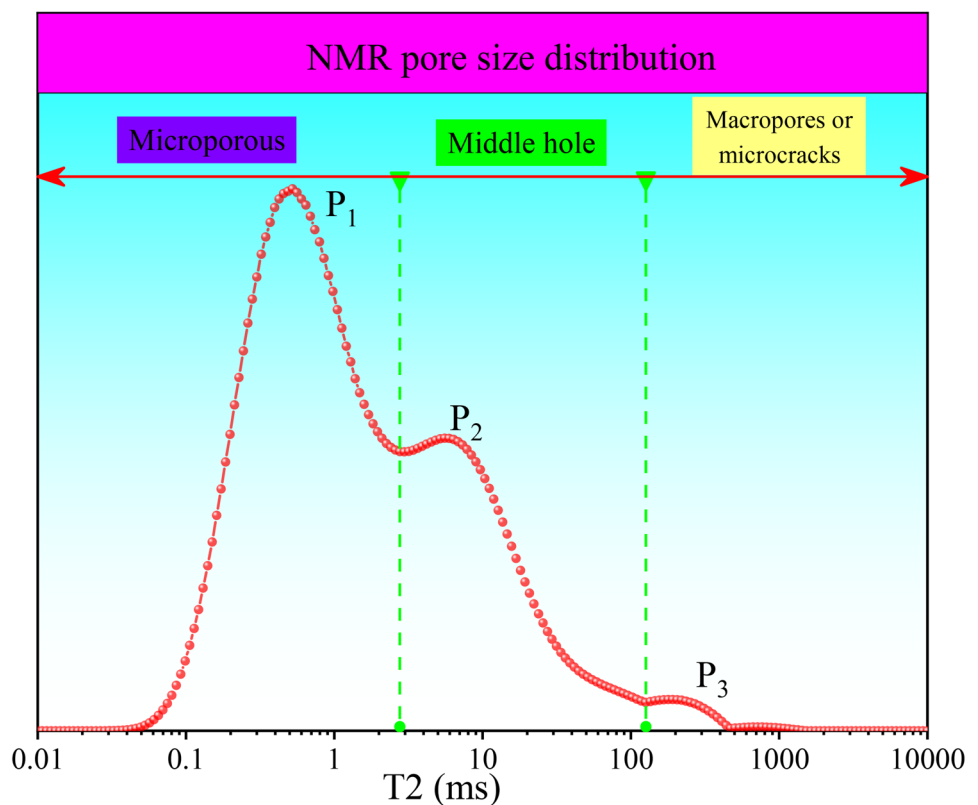
Table 4 Change in the porosity of samples after different numbers of freeze–thaw cycles
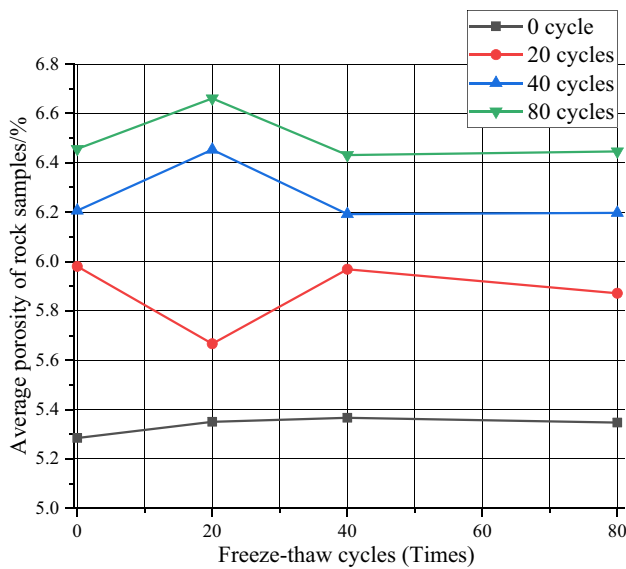
Sample number	Porosity/%			
	0 cycles	20 cycles	40 cycles	80 cycles
G1-1	5.284	5.98	6.206	6.456
G1-2	5.35	5.666	6.453	6.661
G1-3	5.366	5.968	6.192	6.431
Average	5.347	5.871	6.197	6.446

Change in porosity

Table 4 shows the results from the tracking test of three rock samples in the control group, including the porosity of each rock sample and the average porosity of the three rock samples after different numbers of freeze–thaw cycles. At the same time, the porosity test results obtained after different numbers of freeze–thaw cycles are shown in Fig. 7 to visually depict the change in porosity. As the number of freeze–thaw cycles increases, the porosity of each sample increases gradually, but the rate of increase in porosity decreases. According to the previous T_2 spectrum analysis, as the number of freeze–thaw cycles increases, new small pores are generated, the size and number of small pores in the rock mass increase, and the size of large pores increases.

Fig. 6 NMR analysis of the pore size distribution

Fig. 7 Change in the porosity of samples after different numbers of freeze–thaw cycles

The increases in pore size and number correspond to the increase in sandstone porosity.

We quantitatively studied the change in porosity of sandstone before and after freezing and thawing by analyzing the changes in different pores. The NMR data for sandstone are shown in Table 5, which includes the total porosity of the sample and the effective porosity of the corresponding pore type.

The data in the table above were further quantitatively compared and analyzed to specifically study the damage, deterioration, and the change in pore sizes of the rock sample before and after freeze–thaw cycles.

Figure 8 shows the variation in various types of pores in sandstone before and after freezing and thawing. Figure 8a shows an increasing trend in the porosity of micropores with the increase in the number of freeze–thaw cycles. The porosity of mesopores increases during the first 40 cycles and decreases from cycle 40 to 80. The porosity of the macropores or microcracks increases with the number of freeze–thaw cycles. Figure 8b shows that the proportion of micropores in the total pores initially decreases and

then increases with the number of freeze–thaw cycles. The porosity mesopores show the opposite trend. As the number of freeze–thaw cycles increases, the proportion first increases and then decreases. The proportion of macropores or microfractures has no obvious trend, and it shows an increasing trend in porosity.

The small pores inside the sandstone begin to expand into medium or larger pores after the first round of freeze–thaw cycles (20 times), and the mineral particles on the surface of the sandstone begin to peel off after the second round of freeze–thaw cycles (40 times). At the end of the freeze–thaw experiment, the radial end face of the sandstone obviously peels off. Combined with the analysis of the apparent degradation of sandstone during the freezing and thawing process, many micropores are produced when the various pores expand.

In summary, the damage to sandstone caused by freeze–thaw cycles is manifested mainly in the change in pore structure: as each type of pore expands and becomes larger, many new micropores are produced. The increase in the overall porosity of the rock is due mainly to the increase in medium or larger pores. The T_2 spectrum curve shows that the peaks change slightly after freezing and thawing, which also indicates that the change in the pore structure inside the sandstone is attributed to the change in not only the pore structure size but also the number of pores.
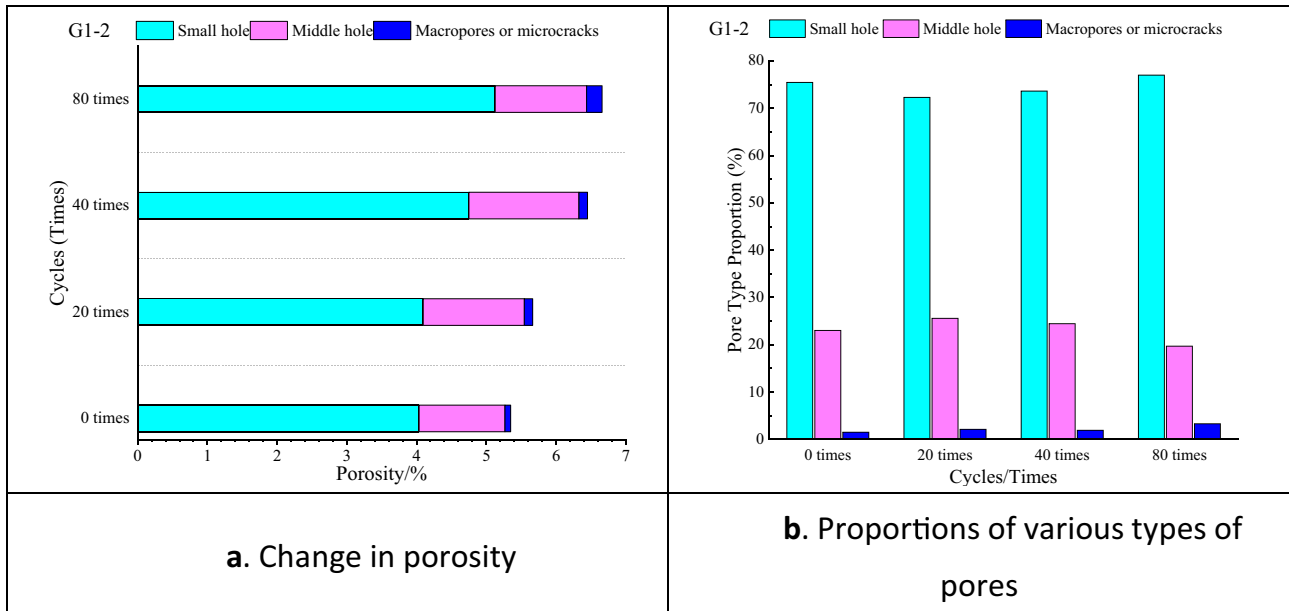
Analysis of the T_2 spectral area

The T_2 spectral area refers to the closed area surrounded by the transverse relaxation time T_2 distribution curve of the NMR and the abscissa, and its size is proportional to the volume of the fluid in the sandstone. When the rock is saturated, the T_2 spectral area can be used to characterize the volume of pores within the rock. Therefore, the change in the area of the T_2 spectrum before and after freezing and thawing reflects the change in the pore volume of the rock (Zhang and Xiao 2006). Accordingly, the first peak in the T_2 spectrum of sandstone is regarded as micropores, the second peak is regarded as mesopores, and the third peak is regarded as macropores or microcracks. Figure 9 shows the

Table 5 Distribution and proportions of different pores in sandstone after different numbers of freeze–thaw cycles

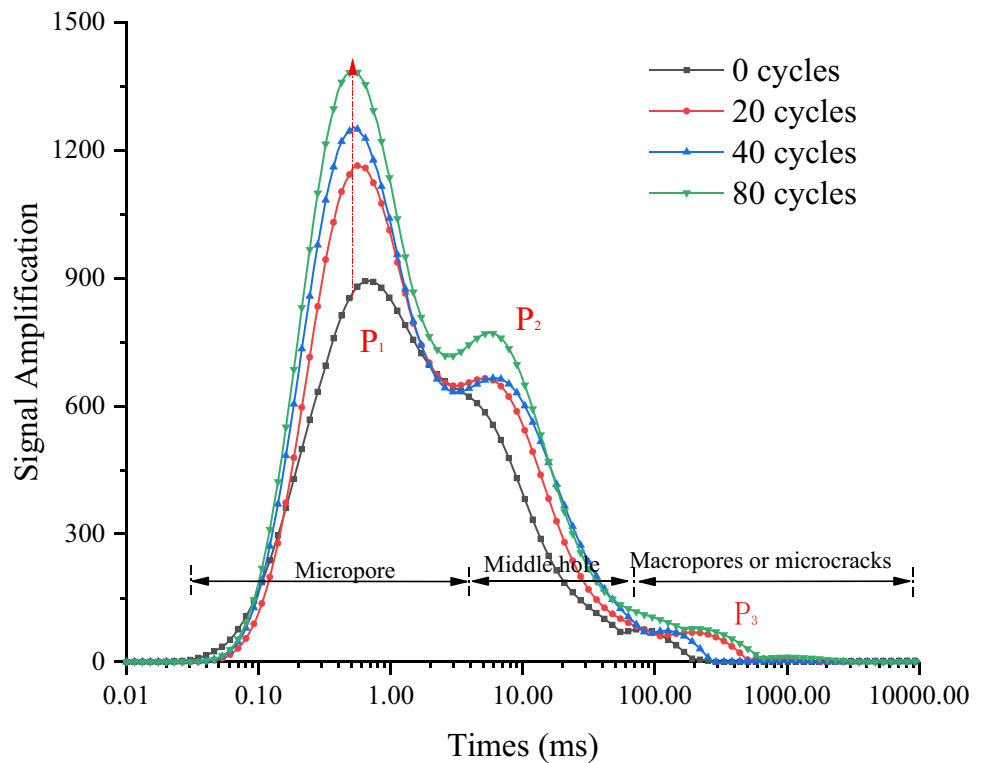| Sample number	Number of cycles	Total porosity/%	Small pores/%	Medium pores/%	Large pores/%	Proportion/%		
						Small pores	Medium pores	Large pores
	0	5.350	4.036	1.232	0.082	75.45	23.03	1.53
G1-2	20	5.666	4.096	1.450	0.120	72.29	25.58	2.12
	40	6.453	4.751	1.578	0.124	73.63	24.46	1.91
	80	6.661	5.128	1.312	0.221	76.99	19.70	3.31

Fig. 8 Changes in various pores in sandstone before and after freezing and thawing. **a** Change in porosity. **b** Proportions of various types of pores

change in the T_2 spectral area of the sandstone after several freeze–thaw cycles. The variation in each peak area of the T_2 spectrum curve is shown in Table 6.

The distribution of signal amplitudes in the T_2 spectrum in Fig. 9 shows that as the number of freeze–thaw cycles increases, the T_2 spectrum distribution shows two trends.

First, as the number of freeze–thaw cycles increases, a left–right movement of the curve appears in the lateral direction, reflecting a decrease in the pore size of the micropores and an increase in the pore size of the macropores or microcracks. Second, the amplitude of the spectral peak curve changes, which is manifested as the upward movement of

Fig. 9 T_2 spectral curve of sandstone after different numbers of freeze–thaw cycles

Table 6 T_2 spectral area and proportion of peaks after different numbers of freeze–thaw cycles

Sample number	Number of cycles	Total area of spectral peaks	First peak	Second peak	Third peak	Proportion/%		
						First peak	Second peak	Third peak
	0	47246.49	34766.68	11413.33	1066.49	73.59	24.16	2.26
G1-2	20	54375.14	38701.69	14519.26	1154.20	71.18	26.70	2.12
	40	61121.44	43237.94	16733.85	1215.57	70.74	27.38	1.99
	80	68577.25	49746.77	17517.30	1313.18	72.54	25.54	1.91

the curve, especially the upward movement of the amplitude of the peak point, indicating that the number of pores is increasing, which is consistent with the NMR T_2 spectrum curve distribution.

As shown in Fig. 10, the spectral area of the sandstone samples changes with the number of freeze–thaw cycles. In general, as the number of freeze–thaw cycles increases, the spectral area increases continuously, indicating that the degree of freeze–thaw damage to the rock mass increases with the increase in the number of freeze–thaw cycles.

The NMR relaxation time T_2 represents the pore size within the rock, where a small T_2 value represents micropores and a large T_2 value represents large pores. The NMR results for different rocks are different, as reflected mainly in the difference in the shape of the T_2 distribution curve. The amplitude of the T_2 spectral signal is related to the pore structure inside the rock. The larger the T_2 amplitude is, the greater the number of pores in the rock is. Therefore, in the NMR T_2 distribution, the spectral area enclosed by the signal amplitude and the T_2 spectrum represents different pore numbers, and the change in amplitude can be used as a measure of the damage to the pore structure. The growth rate of spectral area D_t is defined to represent the rate of change in the pore quantity of sandstone per unit volume during freeze–thaw cycles:

$$\Delta S = S_b - S_a \tag{3}$$

$$D_t = \frac{\Delta S}{S_a} \times 100\% \tag{4}$$

where S_a is the spectral area before freezing and thawing, S_b is the spectral area after freezing and thawing, and ΔS is the change in the spectral area of the corresponding interval before and after freezing and thawing.

Fig. 10 T_2 spectral area of sandstone after different numbers of freeze–thaw cycles
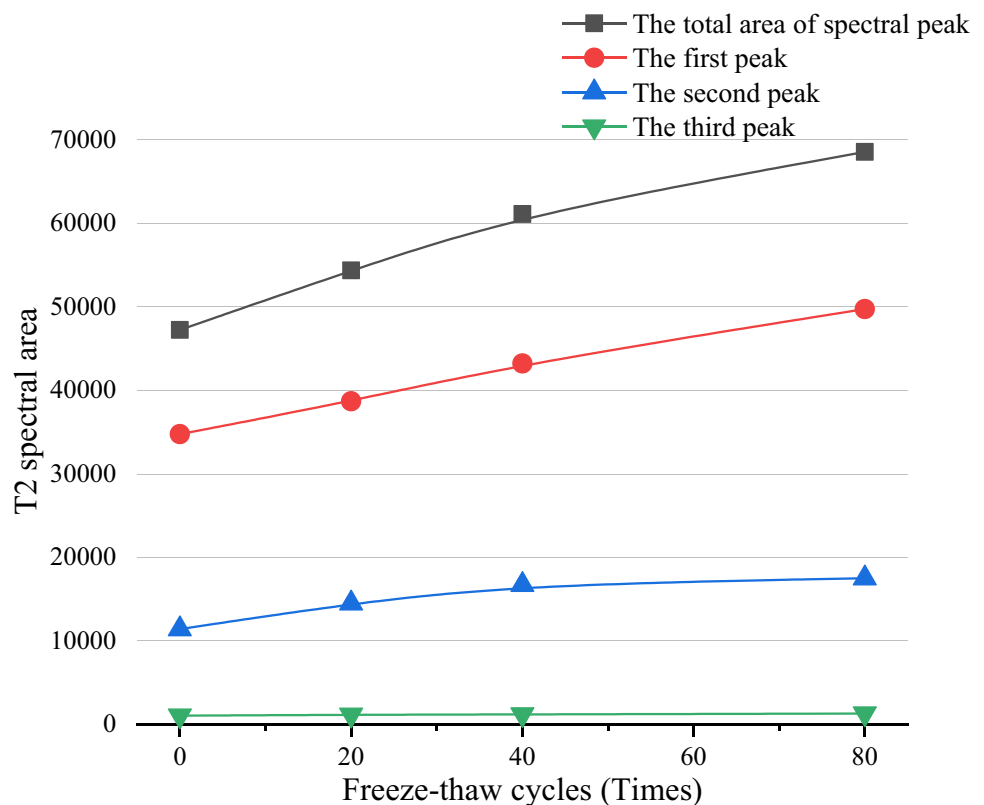
Figure 11 shows the change in the spectral area of various types of pores in the rock sample at different numbers of freeze–thaw cycles. Based on the number of pores before the freeze–thaw cycle, the changes in the types of pores after the cycle were quantitated. The trend of the full pore spectral area and the micropore spectral area of the sandstone samples after freezing and thawing shows that the rate of change in the early stage is relatively fast and gradually stabilizes in the later stage, and the whole process shows continuous growth. Based on the mutual relationship between the growth rates of different types of pores, microcracks inside the rock continuously develop, and micropores are continuously generated. Some of the micropores expand into mesopores and macropores during the freezing and thawing process. Micropores and mesopores play important roles in increasing the number of large pores.

The damage to large pores or microcracks in sandstone always increases, and the increase is relatively slow in the later period. The damage mechanism may be explained by the joint action of hydrostatic pressure theory and fractional ice theory. During freeze–thaw cycles, the water inside the sandstone migrates to the icy surface. Repeated freezing and thawing processes cause the shedding of mineral particles from the surface of the sandstone and the peeling of the surface, leading to intensified damage and increased numbers of macropores or microcracks. The saturated fractures are under two stress states during freeze–thaw cycles, namely the frost heave tensile stress and the overall volume expansion force generated by the frost heave inside the rock.

The aforementioned analysis of the T_2 spectra shows that under the effect of freezing and thawing cycles, the T_2 spectrum moves left and right in the horizontal direction, indicating that the pore structure changes gradually as micropores gradually expand into mesopores or macropores, accompanied by the formation of new, small pores. The overall porosity increases; after the freeze–thaw cycle, the peak value of the T_2 spectra increases, indicating that the various pores in the rock change in both size and quantity.

MRI analysis of microstructural damage

MRI was used to visually observe the evolution of internal pore damage in the rock. The characteristics of the changing internal pore structure of the rock mass after different freeze–thaw cycles are used to explain the freeze–thaw damage process in the rock through the change in the pore distribution indicated by the MRI results.

The experiment used the NMR imaging core device to study the internal pore size distribution of the rock mass after different freeze–thaw cycles, obtaining two-dimensional images of 3 different position planes in the axial direction (cross section) and radial direction (coronal plane) of the rock sample. The saturated core is detected using NMR after freezing and thawing, the water signal in the rock sample is

Fig. 11 Growth rates of T_2 spectral regions of sandstone samples with different pore types after different numbers of freeze–thaw cycles
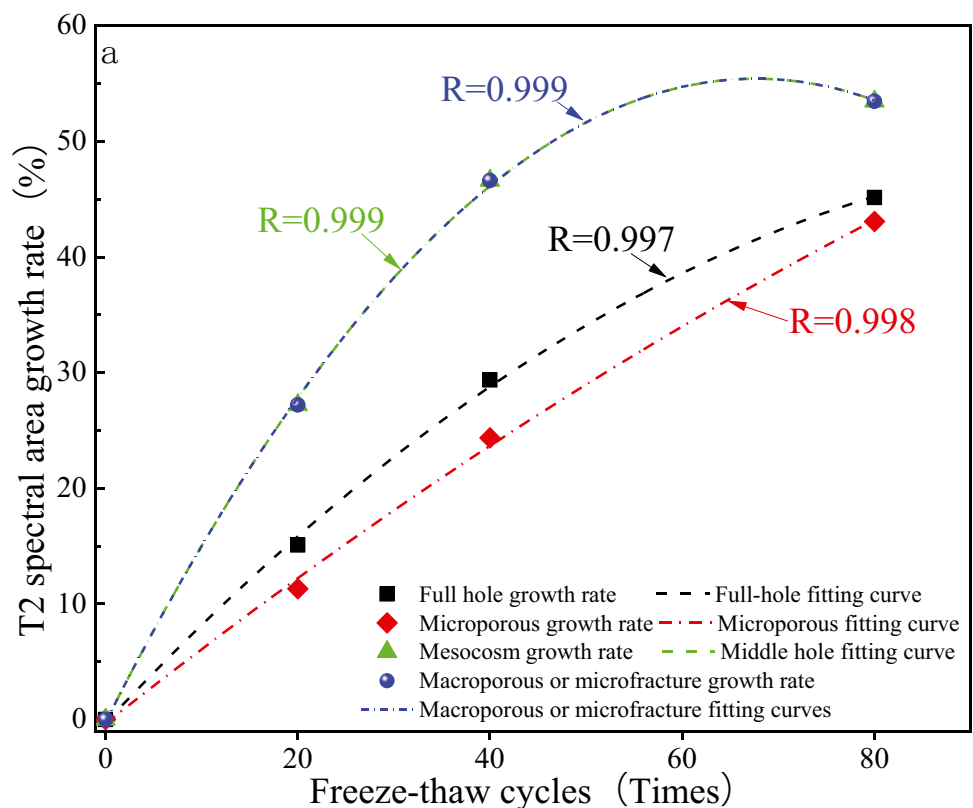
recorded, and the signal is processed and analyzed (see the principle of nuclear MRI for the specific analysis process) to show the damage and degradation of the rock sample induced by the freeze–thaw cycles.

1. Selection of core imaging slices

    MRI cuts the rock core in any direction to obtain the pore distribution and size in the slice at the corresponding position. This experiment is divided into core cross section (a) and coronal plane imaging (b). The pore distribution in different sections is analyzed. A schematic of the position of the specific section is shown in Fig. 12. The slice thickness h of the core cross section is measured as 15 mm for the length of the fracture, and the interval d is measured as 10 mm. We referred to the coordinate orientation of the MRI machine to ensure that the sample was placed in the proper orientation. This approach facilitates the comparative analysis of MRI data after freezing and thawing, and the degree of pore damage in the cross section of the sandstone after different freezing and thawing conditions is directly and clearly obtained from the appearance. The coronal imaging layer thickness h and the layer spacing d are both 10 mm. The sample was placed in the carrier, oriented, and labeled to ensure that it was in the same position every time.
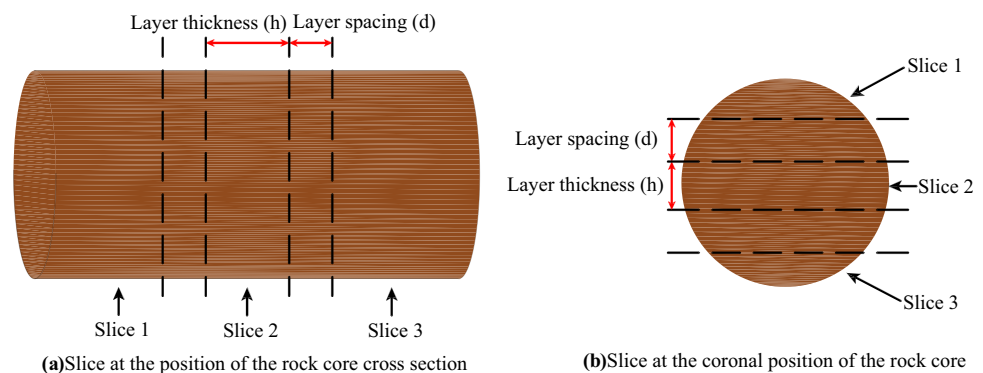
2. Experimental results

    MRI imaging was performed on each group of tracking test samples after different numbers of freeze–thaw cycles. According to the test results, one sample in each group was selected for a comparative analysis of MRI data before and after freezing and thawing. The change in the MRI image directly reflects the degree of damage to the internal pores of the rock mass caused by the freeze–thaw cycle.

    Figure 13 shows the MRI results for sample G1-1 after different numbers of freeze–thaw cycles. For the rock sample with 0 freeze–thaw cycles, the white spots in the figure are relatively small, the brightness is uneven, the number of pores in the cross section is small, mainly

small-sized pores are observed, and the rock contains mainly bound water. The spot brightness in Sect. 1 of the picture is greater than that in other areas, indicating that this part may contain initial microcrack damage. The darker area in the picture indicates that the rock structure is dense. After 20 freeze–thaw cycles, the white spots inside the rock sample become increasingly brighter, and the original macropores or microcracks become brighter. The bright spots in the other images are also brighter and more numerous than the 0-cycle MRI results. After 40 freeze–thaw cycles, the brightness of the rock sample image increases. The size and shape of the pores are clearly visible, and the bright spots on the edge continue to brighten. These changes are related to the degradation of sandstone. As the number of freeze–thaw cycles increases, the sample exhibits particle exfoliation along the radial end surface and an increase in bright spots after imaging. After 80 freeze–thaw cycles, the white spots inside the rock become increasingly brighter, and the distribution becomes increasingly uniform. The area becomes increasingly larger, and the pores are directly connected to one piece. The degree of damage is worsened. The coronal images of different slices also show that the process of freeze–thaw damage to the fractured rock mass entails the continuous evolution of small-sized pores into large-sized pores, accompanied by the generation of new small pores.

    Figure 14 shows the coronal images for sandstone sample G1-1 after different numbers of freeze–thaw cycles. The more freeze–thaw cycles there are, the more white spots inside the rock there are and the larger the area is. Eventually, white spots on the ends and edges increase significantly, the brightness increases, and local damage occurs. In the 0-cycle image, the white spots are less bright, exhibit an uneven distribution, and contain few pores. After 20 freeze–thaw cycles, the brightness of the white spots on the coronal image gradually increases, and their distribution is denser. After 40 freeze–thaw cycles, the brightness of the white spots grows increasingly stronger, and the white spots in local areas increase

Fig. 12 Schematic of the core imaging slice

(a) Slice at the position of the rock core cross section

(b) Slice at the coronal position of the rock core

Fig. 13 Cross-sectional MRI results for sample G1-1 before and after freezing and thawing
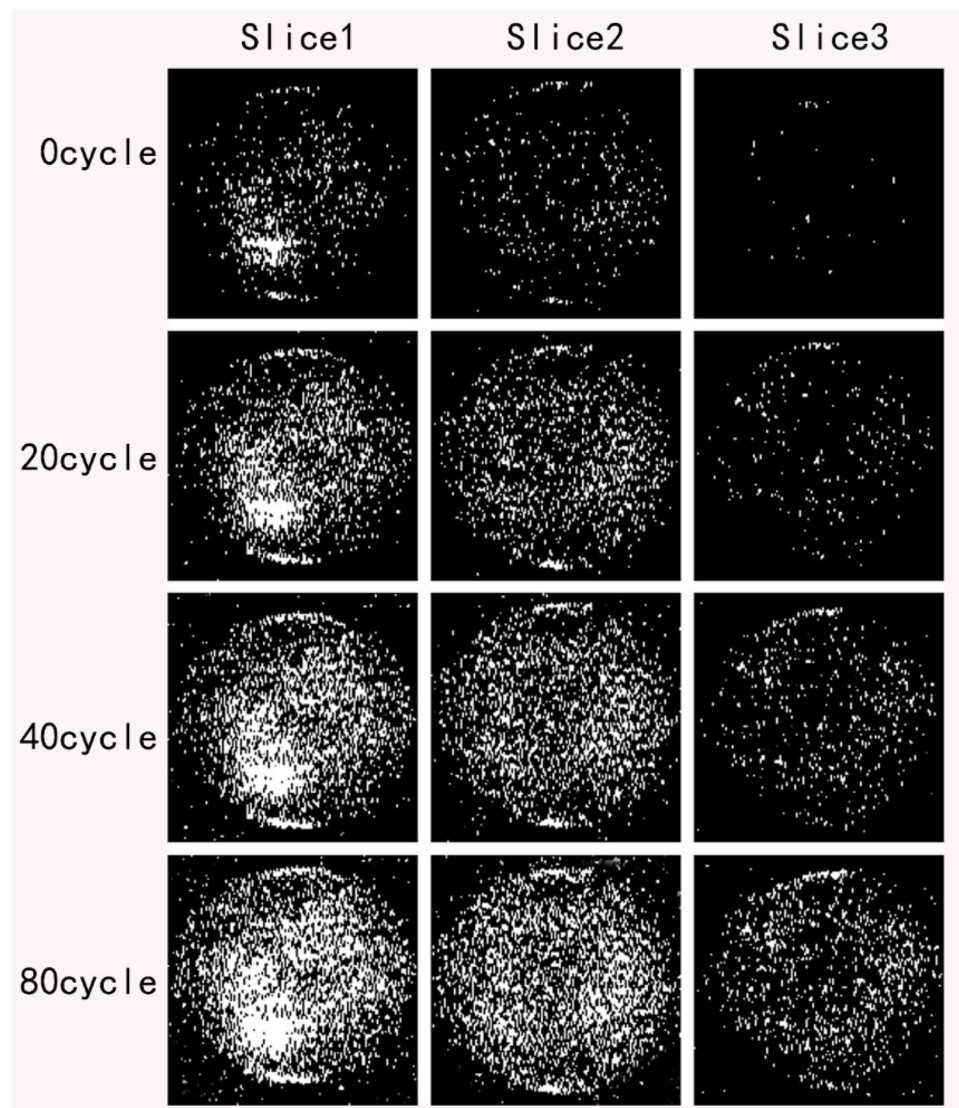
significantly. This result may be due to the increase in the number of freeze–thaw cycles. Freezing and thawing generate holes in the rock surface with incremental ends, leading to the exfoliation of mineral particles on the end face of the rock and an increasing number of micropores. After 80 freeze–thaw cycles, the white spots at the end of the rock become increasingly concentrated, brightness significantly increases, and deterioration at the end of the rock increases substantially, with obvious spalling and an increasing number of small pores. A longitudinal comparative analysis shows that with the increase in the number of freeze–thaw cycles, the brightness area of white spots increases, and the pores inside the rock increase.

A comprehensive analysis of the pore evolution of the cross-sectional and coronal NMR imaging results shows that with the progress of the freeze–thaw cycle,

small pores in the sandstone samples continue to expand into large pores or microcracks. Simultaneously, with the initiation of small pores, obvious particle exfoliation and deterioration occur at the end of the sample, and the outer surface of the sample shows the generation of microholes. The experimental results are directly related to the failure mode of the sandstone appearance, and the results are also consistent.

3. Discussion and analysis

According to the MRI analysis of typical samples, MRI intuitively reflects the process underlying the change in the internal porosity of the rock sample before and after freezing and thawing. Before freezing and thawing, the internal pore structure of the rock is relatively complete, and the distribution of white dots in the initial NMR image is relatively scattered. This pattern

Fig. 14 Sagittal MRI results for sample G1-1 before and after freezing and thawing
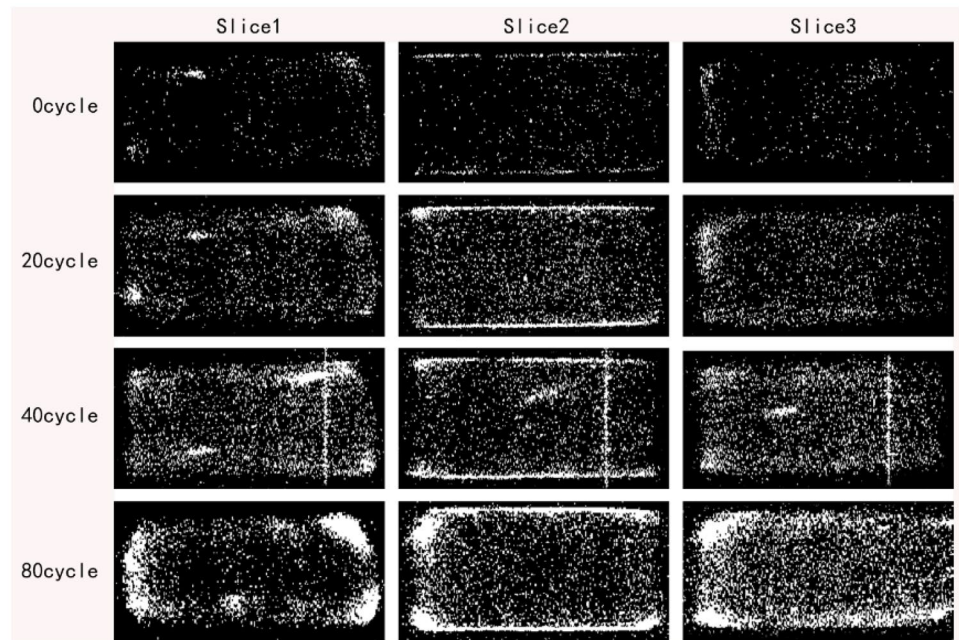
corresponds to the large proportion of small pores analyzed in the T_2 spectrum distribution of the rock NMR. After the freezing and thawing cycle begins, the MRI results shows an increasing number of scattered white spots that are brighter with an increasing uniform distribution, and the corresponding rock porosity increases with the number of freeze–thaw cycles. When the degree of freeze–thaw damage further deteriorates the sample, the white areas in the different sections of the sample are further brightened and enlarged, indicating that the small pores in the rock body continue to evolve into large pores or large cracks after repeated freezing and thawing cycles. The microcracks further penetrate and propagate, and the whole process is accompanied by the generation of small pores. The changes in MRI results are consistent with the change in the core NMR T_2 spectrum distribution.

A comparative analysis of the rock cross-sectional imaging results and the coronal imaging results revealed that the cross-sectional MRI result is partially deformed. The processed image is not a standard circle but slightly deformed because the sandstone sample contains a small amount of ferromagnetic substances (based on an XRF analysis of the sandstone sample, the iron content is approximately 3%), the magnetic field is more sensitive to iron, and not all natural cores can be directly imaged using NMR. Certain differences in the MRI results for the same sample are observed after the same number of freeze–thaw cycles. The signal distribution of the obvious cross section is more obvious, and the white dot distribution is brighter because the MRI results are related to the positioning and gradient field. The basic

principle of MRI has been discussed in detail. Under certain gradient field strength and selected layer thickness conditions, the pulse width is fixed, the cross section layer thickness is 15 mm, and the coronal plane layer thickness is 10 mm. The layer selection gradient is not substantially different from the coronal plane, the pulse width between the two is obviously different, and the received signal also differs. At the same time, due to the inconsistency in the signal quantities of the three slices of the coronal plane, coronal imaging is based on a section in the radial direction, and the result of NMR imaging is an accumulation of all the signal quantities, including the thickness of the selected slice. The cylinder is a curved surface projection. Based on the center plane, the MRI results show that slice 2 is the widest (diameter width), and the signal is the strongest. Slices 1 and 3 have narrow widths, relatively few white spots, and a small number of pores.

According to the distribution characteristics of the NMR T_2 spectrum and the characteristics of the sandstone pore distribution, the approximate distribution times of the three T_2 spectrum peaks are 0.5–2, 8–12, and more than 100 ms. These spectrum peaks correspond to micropores and transition pores (< 100 nm), mesopores (100–1000 nm), and macropores or microcracks, respectively. The changes in the effective pores and spectral areas of each spectral peak in the rock samples after different numbers of freeze–thaw cycles were also examined. The micropore T_2 spectral area of each group of samples increases approximately linearly. The growth rate of the mesoporous T_2 spectral area changes rapidly in the early stage but is relatively flat in the later stage.

Variation in mechanical parameters

Stress–strain curve after freeze–thaw cycling

Figure 15 shows the typical stress–strain curve of sandstone after freezing and thawing.

As shown in Fig. 15, the stress–strain curve of the uniaxial compression experiment of sandstone after freezing and thawing includes six stages.

1. A pore compaction stage: This stage is the initial stage of sample loading, the curve shows an upward concave shape, and the initial stage of deformation shows a significant nonlinear feature. With the increase in the axial load, the pores gradually close and become compact. In this process, the slope of the curve increases with increasing strain. As the number of freeze–thaw cycles increases, the compaction stage of the rock is prolonged.
2. AB elastic deformation stage: After the curve passes point A, the curve maintains an approximately linear change under the action of axial stress, and the slope remains basically unchanged. The deformation characteristic of this stage is the recoverable elastic deformation. As the number of freeze–thaw cycles increases, the slope of this stage decreases, and the elastic modulus also decreases.
3. BC microfracture initiation stage: After elastic deformation reaches point B, stress concentration at the end of the fracture with increasing axial load leads to the generation of new cracks, and a turning point appears on the curve. This stage has a relatively short duration, and the deformation process is irreversible.
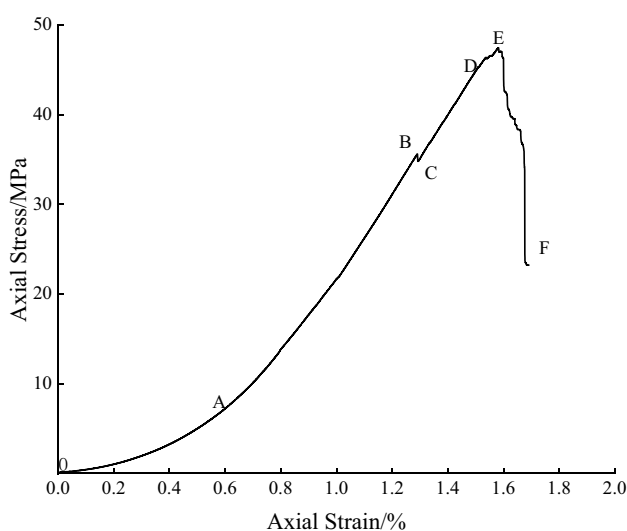
4. CD microcrack stable expansion stage: New microcracks or micropores in the rock expand stably under compressive stress until the rock sample is destroyed. This stage is nonlinear and is categorized as plastic deformation.
5. DE progressive failure stage: The stress concentration effect caused by the axial load is significant at this stage. The weak part of the rock is first destroyed, the stress is redistributed, and the slope of the curve changes significantly until the maximum compressive strength is reached and the rock is completely destroyed.
6. EF postfailure stage: After the sample reaches the maximum compressive strength, the rock is completely broken, and a macroscopic fracture surface appears. The stress–strain curve falls rapidly. After point F, the stress–strain curve tends to be horizontal, which corresponds to the residual strength stage of the rock.

The aforementioned stages are all reflected in the stress–strain curve of sandstone, which well describes the process underlying the change in the stress–strain curve of sandstone after freeze–thaw cycles.

Stress–strain curves after different numbers of freeze–thaw cycles

Repeated freeze–thaw cycles cause fatigue damage to the rock mass. At the micro level, freeze–thaw cycles are characterized by changes in pores. At the macro level, the most direct effect is the weakening of mechanical strength. Both of these aspects are reflected by two important mechanical parameters of rock deformation and strength. The stress–strain curves of the samples after different numbers of freeze–thaw cycles are obtained from the test results, as shown in Fig. 16. In the figure, A, B, C and D represent 0, 20, 40, and 80 cycles, respectively.

1. As shown in Fig. 16, the strength of the rock samples decreases with increasing numbers of freeze–thaw cycles. The strength of the rock sample in the early stage of freeze–thaw cycles (20 cycles) is slightly lower than that in the unfrozen-thawed state, indicating a small degree of damage to the rock sample in the early stage of freezing and thawing. After 80 freeze–thaw cycles, the uniaxial compressive strength of the rock sample decreases significantly. Thus, the rock sample seriously deteriorates due to freeze–thaw damage.
2. In the pore compaction stage, the length of the strain interval corresponding to each curve differs. As the number of freeze–thaw cycles increases, the change in the sample in the compaction stage becomes increasingly obvious, showing that the compaction stage is prolonged, while the elastic deformation stage is shorter.
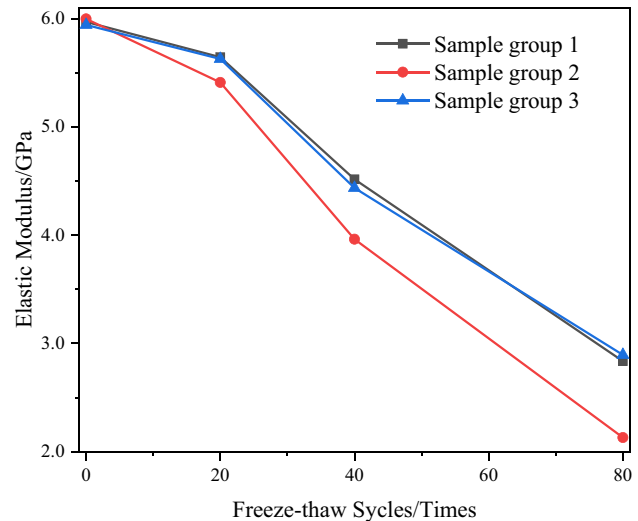

Fig. 15 Stress–strain curve for the uniaxial compression of sandstone after freezing and thawing
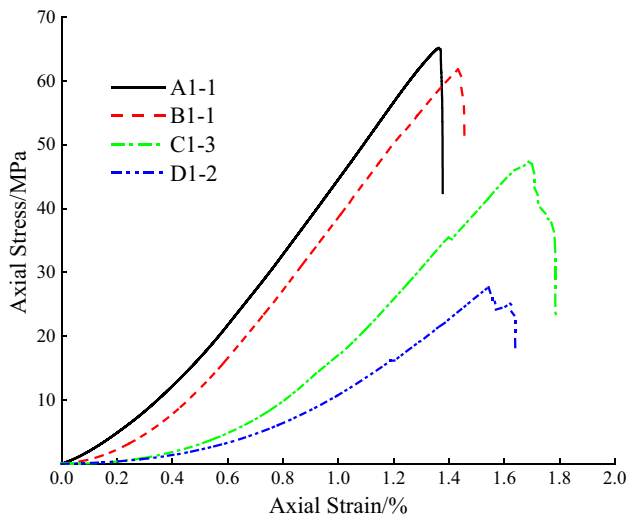
Fig. 16 Stress–strain curves for different numbers of freeze–thaw cycles

Fig. 17 Relationship between the elastic modulus of sandstone and the number of freeze–thaw cycles

The rock undergoes uniaxial compression after different numbers of freeze–thaw cycles. Repeated freeze–thaw cycles will increase the number of micropores in the rock. The more freeze–thaw cycles that occur, the more obvious the development of micropores. During the uniaxial compression test under the loading of axial stress, the micropores in the rock close, and the axial strain of the rock sample increases accordingly. However, when the rock sample reaches the elastic stage, because the initial fracture is relatively developed, elastic deformation occurs under very small stresses, and the corresponding elastic deformation range shortens.

3. As the number of freeze–thaw cycles increases, the failure mode of the rock sample changes. Before and in the early stage of freeze–thaw cycling, the failure of the sample shows obvious brittle failure. After reaching peak stress, damage occurs suddenly. With the increase in the number of freeze–thaw cycles, the slope of the stress–strain curve becomes relatively gentle, and the postpeak stage shows a certain plastic deformation, which is a form of ductile failure, indicating that the brittleness of the sandstone is reduced and the plasticity is enhanced after freeze–thaw cycles.

4. The elastic modulus of the rock sample and the linear section on the stress–strain curve show a decreasing trend with increasing numbers of freeze–thaw cycles.

Relationship between the number of freeze–thaw cycles and the elastic modulus of sandstone

As shown in Fig. 17, the elastic modulus of sandstone decreases with the increase in the number of freeze–thaw cycles, and the rate of the decrease gradually accelerates.

Discussion

Attenuation of the mechanical properties of sandstone undergoing freezing and thawing cycles

Constitutive relation of rock damage during freeze–thaw cycles with loading

Under static loading, the material is assumed to be subjected to force F before freezing and thawing, causing a certain amount of damage. The initial section area of the rock is A, the area after freeze–thaw damage is A^*, the effective area is $\dot{A} = A - A^*$, the total stress is $\sigma = F/A$, and the effective stress is $\dot{\sigma} = F/\dot{A}$. The effective area of rock damage after freeze–thaw cycles remains unchanged, according to the strain equivalent principle proposed by Professor Lemaitre (Lemaitre and Dufailly 1987). Under uniaxial loading, the strain caused by the total stress on the damaged material is equivalent to the strain caused by the effective stress on the nondestructive material, namely:

$$\varepsilon = \sigma/\dot{E} = \dot{\sigma}/E \tag{5}$$

where E is the elastic modulus of the unfrozen rock and $\dot{E}$ is the effective elastic modulus of the rock after freezing and thawing.

A rock mass is a complex geological material that contains many macroscopic and mesoscopic defects. The elastic modulus of rock is very difficult to obtain during the actual measurement process. Therefore, according to the strain equivalent principle proposed by Zhang et al. (2003), the material is subjected to the force F, and the damage is

expanded. If any two of the damage states occur, the strain caused by the effective stress of the material in the first damage state acting on the second damage state is equivalent to the strain caused by the effective stress of the material in the second damage state acting on the first damage state. The specific equation is:

$$F = \sigma' \times A' = \sigma'' \times A'' \tag{6}$$

where σ' is the effective stress in the first damage state; A' is the effective bearing area in the first damage state; σ'' is the effective stress in the second damage state; and A'' is the effective bearing area in the second damage state.

The principle of strain equivalence after promotion is:

$$\varepsilon = \sigma'/E'' = \sigma''/E' \tag{7}$$

where E' and E'' are the elastic moduli of two different damage states.

Therefore, according to Formula (7), the damage to rocks before and after freeze–thaw cycling is defined as the first and second damage states, respectively:

$$\sigma_0 A_0 = \sigma_n A_n \tag{8}$$

$$D_n = 1 - \frac{A_n}{A_0} \tag{9}$$

where σ_0 is the effective stress before the rock is frozen and thawed, MPa; A_0 is the effective bearing area before the rock is frozen and thawed, m^2; σ_n is the effective stress after the rock is frozen and thawed, MPa; A_n is the effective bearing area after the rock is frozen and thawed, m^2; and D_n is the damage variable after the rock has undergone freeze–thaw cycles.

From Eqs. (8) and (9), the constitutive relation between the elastic modulus and the freeze–thaw damage to rock materials in two states is written as follows according to the generalized strain equivalence principle:

$$E_n = E_0(1 - D_n) \tag{10}$$

$$\sigma_n = E_0(1 - D_n)\varepsilon_n \tag{11}$$

The extended principle of strain equivalence is used again, and the constitutive relationship between damage to rock undergoing freeze–thaw cycling and loading is obtained as follows:

$$\sigma = E_0(1 - D_t)\varepsilon \tag{12}$$

In the formula:

$$D_t = D + D_n - DD_n \tag{13}$$

where D_t is the cumulative damage variable for the rock freeze–thaw load.

Equation (13) shows that under the combined action of freeze–thaw cycles and loading, the degree of damage to rocks becomes increasingly serious and has obvious nonlinear characteristics. The coupling effect of freeze–thaw cycles and load reduces the cumulative damage to rocks.

Analysis of mechanical strength degradation

Figure 18 shows the relationship between the peak strength loss rate of sandstone and the number of freeze–thaw cycles.

The rate of the loss in the sandstone peak strength is calculated using the following equation:

$$\eta = \frac{F_0 - F(n)}{F_0} \times 100\% \tag{14}$$

where F_0 is the uniaxial compressive strength of sandstone before freeze–thaw cycling, MPa, and $F(n)$ is the uniaxial compressive strength of sandstone after n freeze–thaw cycles, MPa.

Figure 18 shows that the loss rate of the uniaxial compressive strength of sandstone increases with increasing numbers of freeze–thaw cycles, indicating that the uniaxial compressive strength of sandstone is related to the number of freeze–thaw cycles. In the first 20 freeze–thaw cycles, the rate of sample strength loss is small, whereas the loss rate significantly increases after 20 cycles. The reason is that sandstone is a porous rock. During freezing in the saturated state, the water–ice phase transformation will expand the volume and produce the frost heaving force. During the cooling process, the temperature of the rock is transferred from the outside to the inside. Due to the existence of
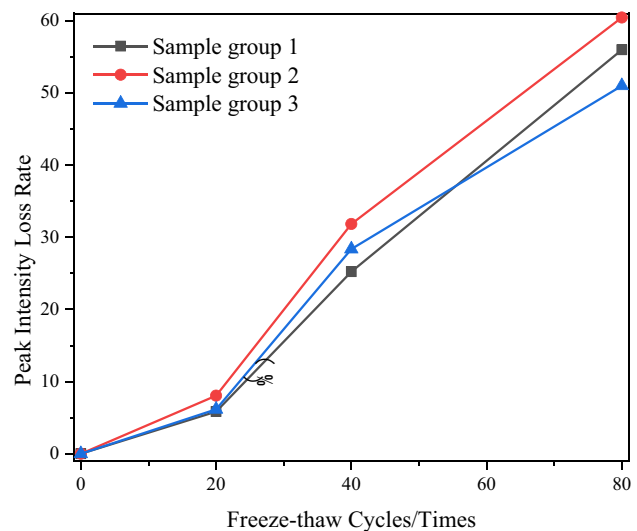
Fig. 18 Relationship between the peak strength loss rate of sandstone and the number of freeze–thaw cycles

the condensing potential energy, the water inside the rock migrates to the surface of the rock. During the melting process, the migration of temperature and moisture shows the opposite pattern. Repeated freezing and thawing will cause the bonds between the mineral particles on the surface of the rock to decrease, and flaking of the surface mineral particles occurs. As the number of freeze–thaw cycles increases, the strength and elastic modulus of the rock are substantially reduced.

Model of sandstone strength degradation after freezing and thawing

1. Establishment of a sandstone strength degradation model after freezing and thawing based on changes in the relative elastic modulus

We assumed that the peak strength of sandstone after n freeze–thaw cycles is $F(n)$, which is a differentiable function, and the peak strength of sandstone without freeze–thaw cycles is F_0. Then, from n to $(n + \Delta n)$ freeze–thaw cycles, the peak strength loss rate of sandstone is:

$$\frac{F(n) - F(n + \Delta n)}{F(n)} = \alpha \Delta n \ (\alpha > 0) \tag{15}$$

This formula is transformed as follows:

$$\frac{dF(n)}{dn} = \alpha F(n) \tag{16}$$

The integral of Eq. (16) is calculated as follows:

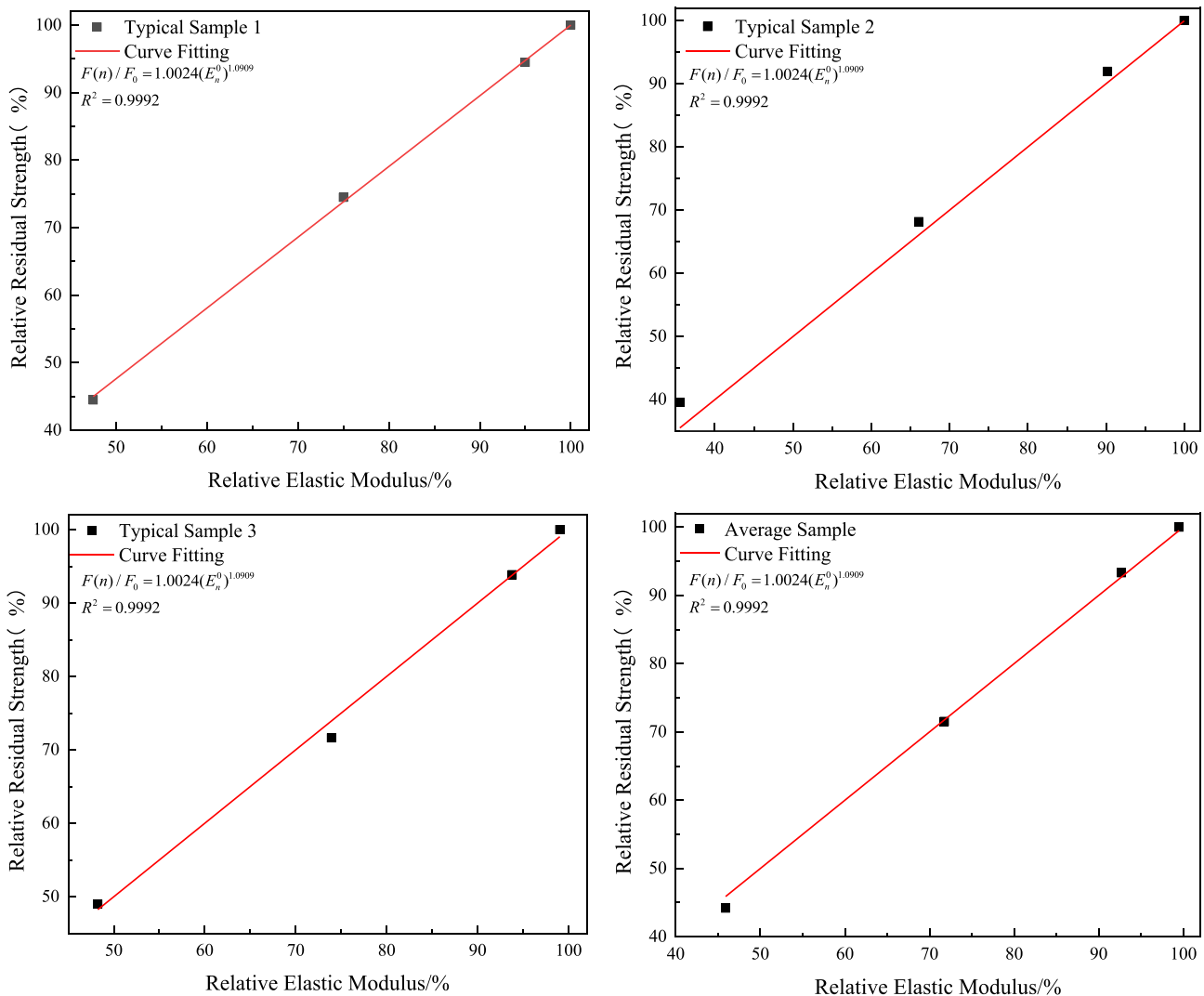$$\frac{F(n)}{F_0} = \exp(\alpha n) \tag{17}$$

Fig. 19 Relationship between the relative residual peak strength and relative elastic modulus of sandstone after freeze–thaw cycles

As the number of freeze–thaw cycles increases, the elastic modulus of sandstone gradually decreases (as shown in Fig. 17), similar to the peak strength. Correspondingly, the loss rate of the elastic modulus of sandstone is also proportional to the number of freeze–thaw cycles. We assumed that the uniaxial compressive elastic modulus of sandstone after n freezing–thawing cycles is $E_n(n)$, which is a continuous differentiable function, and the elastic modulus of unfreeze–thaw is E_0. Then, from n to $(n + \Delta n)$ freeze–thaw cycles, the loss rate of the uniaxial compressive elastic modulus of sandstone is calculated as follows:

$$\frac{E_n - E_{(n+\Delta n)}}{E_n} = \beta \Delta n \ (\beta > 0) \tag{18}$$

This formula is transformed as follows:

$$\frac{dE_n}{dn} = \beta E_n \tag{19}$$

The integral of Eq. (19) is calculated using the following formula:

$$\frac{E_n}{E_0} = \exp(\beta n) \tag{20}$$

The following equation is obtained by combining Eqs. (19) and (20):

$$\frac{F(n)}{F_0} = \left(\frac{E_n}{E_0}\right)^{\alpha/\beta} \tag{21}$$

Let $E_n^0 = E_n/E_0, \phi = \alpha/\beta$ be the conversion coefficient of the relative peak strength and relative elastic modulus of sandstone. The correction factor λ is introduced to correct the equation. Then, the aforementioned equation becomes:

$$\frac{F(n)}{F_0} = \lambda(E_n^0)^\phi \tag{22}$$

Equation (22) shows that the relative peak strength and relative elastic modulus of sandstone undergoing freeze–thaw cycles obey the power function relationship. As the uniaxial compression peak strength loss rate and the elastic modulus are not completely proportional to the number of freeze–thaw cycles, the model shown above should be fitted and corrected according to the relevant data to obtain specific values for λ and ϕ.

2. Fitting relationship between the relative residual peak strength and relative elastic modulus of sandstone after freeze–thaw cycles

According to the aforementioned derivation, the power function model $y = ax^b$, which is consistent with the model, is selected to fit the variation in the relative residual peak strength and relative elastic modulus of sandstone after freeze–thaw cycles. The fitting results are shown in Fig. 19. The figure shows a good correlation between the relative residual peak strength and the relative elastic modulus of sandstone. Therefore, the residual peak strength is evaluated according to the relative elastic modulus of sandstone after freeze–thaw cycles. The fitting parameters λ, ϕ, and R^2 of the sandstone relative peak strength and relative elastic modulus after freeze–thaw cycles are 1.0025, 1.0909, and 0.992, respectively.

Conclusions

Studying the deterioration of rock masses during freeze–thaw cycles is important to obtain a deeper understanding of rock engineering failure mechanisms in cold regions. The microscopic damage evolution law after freeze–thaw cycles was revealed using NMR, and several conclusions were drawn from the results.

1. With the increase in the number of freeze–thaw cycles, the mass of the rock sample initially appears to increase. As the number of freeze–thaw cycles increases, the appearance of the rock sample shows different degrees of mineral particle spalling, the quality of the rock sample decreases, and the deterioration damage caused by freezing and thawing is aggravated.

2. With the increase in the number of freeze–thaw cycles, the T_2 spectral area of the micropores of the sample increases approximately linearly. The T_2 spectral area growth rate of the mesopores changes rapidly in the early stage and is relatively mild in the later stage. The growth rate of macropores or microcracks is fast in the early stage and relatively stable in the later stage. The micropores continue to expand into large pores as the number of freeze–thaw cycles increases, while new small pores are continuously generated, and rock damage becomes increasingly serious.

3. The uniaxial compressive stress–strain curve is approximately divided into six stages. As the number of freeze–thaw cycles increases, the deformation at each stage differs. The compressive strength and elastic modulus of sandstone are reduced to different extents. The frost resistance coefficient of sandstone decreases, but the deformation of the compaction stage of the typical stress–strain curve increases.

4. The changes in the NMR imaging results are consistent with the changes in the NMR T_2 spectrum distribution. The whole process manifests as the generation and development of microcracks, the intensified expansion of microcracks, the generation and development of

macropores, the expansion and penetration of macropores, and finally, rock damage.

5. 5. Freeze–thaw cycles exert a certain effect on exacerbating damage to the rock mass. With the increase in the number of freeze–thaw cycles, the uniaxial compressive strength and elastic modulus of the rock mass are continuously reduced. The loss rate of the uniaxial compressive peak strength of the rock mass under the influence of freeze–thaw cycles is related to the loss rate of the elastic modulus. The relationship between the relative residual uniaxial compressive peak strength and the relative elastic modulus is derived as follows: $F(n)/F_0 = \lambda (E_n^0)^\phi$. The data are fitted through experiments, producing a high surface fitting degree.

References

Abdolghanizadeh K, Hosseini M, Saghafiyazdi M (2020) Effect of freezing temperature and number of freeze–thaw cycles on mode i and mode ii fracture toughness of sandstone. Theor Appl Fract Mech 105:102428. https://doi.org/10.1016/j.tafmec.2019.102428

Al-Omari A, Beck K, Brunetaud X, Torok Al-Mukhtar M (2015) Critical degree of saturation: a control factor of freeze–thaw damage of porous limestones at Castle of Chambord. Eng Geol 185:71–80. https://doi.org/10.1016/j.enggeo.2014.11.018

Coates G, Xiao L, Prammer M (2007) NMR logging principles and application. Petroleum Industry Press, Beijing, pp 6–7

Gao F, Xiong X, Zhou K, Li J, Shi C (2019) Strength deterioration model of saturated sandstone under freeze-thaw cycles. Rock Soil Mech 40(3):926–932. https://doi.org/10.16285/j.rsm.2017.1886

Guo L, Yu Q, Yin N, Zhang D, Zhang D, Ren X, You Y, Zhang Z, Hu B, Chen S (2022) Effect of freeze–thaw cycle on hydraulic conductivity of compacted clayey soil. J Mt Sci 19(2):606–614. https://doi.org/10.1007/s11629-021-6683-9

Ishikawa T, Kawabata S (2016) Influence of freeze-thaw on the mechanical behavior of the granular base and fatigue life of pavement structures in Japan. Geo-china International Conference

Jamshidi A, Nikudel MR, Khamehchiyan M (2016) Evaluation of the durability of gerdoee travertine after freeze–thaw cycles in fresh water and sodium sulfate solution by decay function models. Eng Geol 202:36–43. https://doi.org/10.1016/j.enggeo.2016.01.004

Kellerer-Pirklbauer A (2017) Potential weathering by freeze-thaw action in alpine rocks in the european alps during a nine year monitoring period. Geomorphology 296:113–131. https://doi.org/10.1016/j.geomorph.2017.08.020

Lemaitre J, Dufailly J (1987) Damage measurements. Eng Fract Mech 28(5–6):643–661. https://doi.org/10.1016/0013-7944(87)90059-2

Li J (2012) Experiment study on deterioration mechanism of rock under the conditions of freezing-thawing cycles in cold regions based on NMR technology. Central South University, Changsha

Li J, Kaunda R, Zhu L, Zhou K, Gao F (2019a) Experimental study of the pore structure deterioration of sandstones under freeze-thaw cycles and chemical erosion. Adv Civ Eng. https://doi.org/10.1155/2019/9687843

Li J, Zhou K, Liu W, Deng H (2016) NMR research on deterioration characteristics of microscopic structure of sandstones in freeze–thaw cycles. Chin J Nonferrous Met 26(11):2997–3003. https://doi.org/10.1016/S1003-6326(16)64430-8

Li J, Zhu L, Zhou K, Chen H, Shen Y (2021) Non-linear creep damage model of sandstone under freeze-thaw cycle. J Cent South Univ 28(3):954–967. https://doi.org/10.1007/s11771-021-4656-3

Li X, Qu D, Luo Y, Ma R, Xu K, Wang G (2019b) Damage evolution model of sandstone under coupled chemical solution and freeze-thaw process. Cold Reg Sci Technol 162:88–95. https://doi.org/10.1016/j.coldregions.2019.03.012

Li Y, Tang D, Elsworth D, Hao X (2014) Characterization of coalbed methane reservoirs at multiple length scales: a cross-section from southeastern ordos basin, China. Energy Fuels 28(9):5587–5595. https://doi.org/10.1021/ef500449s

Li Z, Yang G, Liu H (2020) The influence of regional freeze–thaw cycles on loess landslides: analysis of strength deterioration of loess with changes in pore structure. Water 12(11):3047. https://doi.org/10.3390/w12113047

Lindner F, Wassermann J, Igel H (2021) Seasonal freeze-thaw cycles and permafrost degradation on Mt. Geophys Res Lett, Zugspitze (German/Austrian Alps) revealed by Single-station seismic monitoring. https://doi.org/10.1029/2021GL094659

Liu C, Wang D, Wang Z, Ke B, Yu S (2021a) Dynamic splitting tensile test of granite under freeze-thaw weathering. Soil Dyn Earthq Eng 140:106411. https://doi.org/10.1016/j.soildyn.2020.106411

Liu H, Yang G, Yun Y, Lin J, Ye W, Zhang H, Zhang Y (2020a) Investigation of sandstone mesostructure damage caused by freeze-thaw cycles via ct image enhancement technology. Adv Civ Eng. https://doi.org/10.1155/2020/8875814

Liu H, Yuan X, Xie T (2019a) A damage model for frost heaving pressure in circular rock tunnel under freezing-thawing cycles. Tunn Undergr Space Technol 83:401–408. https://doi.org/10.1016/j.tust.2018.10.012

Liu Q, Chen W, Guo J, Li R, Li X (2021b) Fractional stress relaxation model of rock freeze-thaw damage. Hindawi Limited. https://doi.org/10.1155/2021/3936968

Liu T, Wang Y, Zhou K, Gao F, Xie S (2019b) Research on the mechanical properties and nmr characteristics of cement mortar during freeze-thaw cycles. Adv Civ Eng. https://doi.org/10.1155/2019/6805480

Liu T, Zhang C, Cao P, Zhou K (2020b) Freeze-thaw damage evolution of fractured rock mass using nuclear magnetic resonance technology. Cold Reg Sci Technol 170:102951. https://doi.org/10.1016/j.coldregions.2019.102951

Liu T, Zhang C, Li J, Zhou K, Ping C (2021c) Detecting freeze–thaw damage degradation of sandstone with initial damage using nmr technology. Bull Eng Geol Env 80(6):4529–4545. https://doi.org/10.1007/s10064-021-02242-1

Luo X, Jiang N, Fan X, Mei N, Luo H (2015) Effects of freeze-thaw on the deterurination and application of parameters of slope rock mass in cold regions. Cold Reg Sci Technol 110:32–37. https://doi.org/10.1016/j.coldregions.2014.11.002

Meng Y, Jing H, Yuan L, Zhang L (2022) Numerical investigation on the effect of bedding plane properties on mode i fracture characteristics of mudstone with fem-czm method. Bull Eng Geol Env 81(1):1–18. https://doi.org/10.1007/s10064-021-02515-9

Momeni A, Abdilor Y, Khanlari G, Heidari M, Sepahi A (2016) The effect of freeze–thaw cycles on physical and mechanical properties of granitoid hard rocks. Bull Eng Geol Env 75(4):1649–1656. https://doi.org/10.1007/s10064-015-0787-9

Park J, Hyun C, Park H (2015) Changes in microstructure and physical properties of rocks caused by artificial freeze-thaw action. Bull Eng Geol Env 74(2):555–565. https://doi.org/10.1007/s10064-014-0630-8

Park K, Kim K, Lee K, Kim D (2020) Analysis of effects of rock physical properties changes from freeze-thaw weathering in

Ny-angstrom lesund region: Part 1-Experimental Study. Appl Sci 10(5):1707. https://doi.org/10.3390/app10051707

Peng J, Wong LNY, Liu G, et al. (2019) Influence of initial micro-crack damage on strength and micro-cracking behavior of an intrusive crystalline rock. Bull Eng Geol Environ 78: 2957–2971. https://doi.org/10.1007/s10064-018-1317-3

Sokhansefat G, Moradian M, Finnell M, Behravan A, Ley MT, Lucero C, Weiss J (2020) Using X-ray computed tomography to investigate mortar subjected to freeze-thaw cycles. Cem Concr Compos 108:103520. https://doi.org/10.1016/j.cemconcomp.2020.103520

Su Z, Geng K, Zhou F, Sun J, Yu H (2021) Influence of freeze-thaw cycles on acoustic emission characteristics of granite samples under triaxial compression. Adv Civ Eng 3:1–11. https://doi.org/10.1155/2021/5571680

Wang B, Pan J, Fang R, Wang Q (2020a) Damage model of concrete subjected to coupling chemical attacks and freeze-thaw cycles in saline soil area. Constr Build Mater 242(6):118205. https://doi.org/10.1016/j.conbuildmat.2020.118205

Wang J, Liu Y, Tang D (2021a) Influence of freeze-thaw cycles on water content properties of silty clay in xuchang. IOP Conf Ser Earth Environ Sci 772(1):012104. https://doi.org/10.1088/1755-1315/772/1/012104

Wang J, Wang Q, Lin S, Han Y, Wang N (2020b) Relationship between the shear strength and microscopic pore parameters of saline soil with different freeze-thaw cycles and salinities. Symmetry 12(10):1709. https://doi.org/10.3390/sym12101709

Wang L, Chen W, Tan X, Tan X, Zhang X (2019) Numerical investigation on the stability of deforming fractured rocks using discrete fracture networks: a case study of underground excavation. Bull Eng Geol Environ 79:133–151. https://doi.org/10.1007/s10064-019-01536-9

Wang Y, Zhang B, Li B, Li C (2021b) A strain-based fatigue damage model for naturally fractured marble subjected to freeze-thaw and uniaxial cyclic loads. Int J Damage Mech 30(10):1594–1616. https://doi.org/10.1177/10567895211021629

Xu P, Wu Y, Wang Z, Huang L (2020) Distribution laws of freeze-thaw cycles and unsaturated concrete experiments in cold-region tunnels. Cold Reg Sci Technol 172:102985. https://doi.org/10.1016/j.coldregions.2019.102985

Yao Y, Liu D, Yao C, Tang D, Tang S, Huang W (2010) Petrophysical characterization of coals by low-field nuclear magnetic resonance (NMR). Fuel 89(7):1371–1380. https://doi.org/10.1016/j.fuel.2009.11.005

Yuan J, Ye C, Yang J, Xie Z, Liu J, Wang S, Liu Y (2021) Experimental and numerical investigation on the deterioration mechanism for grouted rock bolts subjected to freeze–thaw cycles. Bull Eng Geol Env 80:5563–5574. https://doi.org/10.1007/s10064-021-02279-2

Zhang Q, Yang G, Ren J (2003) A new discussion on rock damage variables and constitutive equations. Chin J Rock Mech Eng 22(1):30–34. https://doi.org/10.3321/j.issn:1000-6915.2003.01.005

Zhang Y, Xiao L (2006) Experimental study on nuclear magnetic resonance characteristics of rock under uniaxial loading. Nucl Electron Detect Technol 26(6):731–734. https://doi.org/10.1016/S1872-2040(06)60004-2

Zhou K, Su S, Hu Z, Li J, Yang Z (2015) NMR experimental study on unloading of marble under different initial damages. Rock Soil Mech 36(8):2144–2150. https://doi.org/10.16285/j.rsm.2015.08.003

Zhou L, Ma Z, Xie H, Yang W, Zheng H (2022) Numerical simulation experimental study of the deformation and failure of granite with multiaxial tension. Processes 10(5):949. https://doi.org/10.3390/pr10050949

Zhou X, Li C, Zhou L (2020) The effect of microstructural evolution on the permeability of sandstone under freeze-thaw cycles. Cold Reg Sci Technol 177:103119. https://doi.org/10.1016/j.coldregions.2020.103119